

BEAM INDUCED HEATING ANALYSIS UPDATE FOR THE EIC VACUUM CHAMBER COMPONENTS

M. Sangroula

September 2023

Electron-Ion Collider
Brookhaven National Laboratory

U.S. Department of Energy

USDOE Office of Science (SC), Nuclear Physics (NP) (SC-26)

Notice: This technical note has been authored by employees of Brookhaven Science Associates, LLC under Contract No. DE-SC0012704 with the U.S. Department of Energy. The publisher by accepting the technical note for publication acknowledges that the United States Government retains a non-exclusive, paid-up, irrevocable, world-wide license to publish or reproduce the published form of this technical note, or allow others to do so, for United States Government purposes.

DISCLAIMER

This report was prepared as an account of work sponsored by an agency of the United States Government. Neither the United States Government nor any agency thereof, nor any of their employees, nor any of their contractors, subcontractors, or their employees, makes any warranty, express or implied, or assumes any legal liability or responsibility for the accuracy, completeness, or any third party's use or the results of such use of any information, apparatus, product, or process disclosed, or represents that its use would not infringe privately owned rights. Reference herein to any specific commercial product, process, or service by trade name, trademark, manufacturer, or otherwise, does not necessarily constitute or imply its endorsement, recommendation, or favoring by the United States Government or any agency thereof or its contractors or subcontractors. The views and opinions of authors expressed herein do not necessarily state or reflect those of the United States Government or any agency thereof.

BEAM INDUCED HEATING ANALYSIS UPDATE FOR THE EIC VACUUM CHAMBER COMPONENTS*

M. Sangroula[†], J. Bellon, M. Blaskiewicz, A. Blednykh, P. Braunius, B. Gallagher, D. Gassner, K. Hamdi, C. Hetzel, D. Holmes, F. Micolon, C. Liu, S. Verdu-Andres
Brookhaven National Laboratory, Upton, NY 11973, USA

Abstract

One of the challenges of designing the Electron-Ion Collider (EIC) is to mitigate beam-induced heating due to the intense electron and hadron beams. Heating of the ESR vacuum chamber components is mainly due to beam-induced resistive wall (RW) losses and synchrotron radiation. For the HSR heating is mainly due to large radial offsets and heat conduction from room temperature to cryogenic temperature for cryo-components. In this paper, we provide an update on the beam-induced heating and thermal analysis of some critical ESR vacuum chamber components, such as the ESR Large Angle Bremsstrahlung Monitor (LABM). We also provide a similar update for critical HSR vacuum components, including the cryo-cooled BPM button assembly, beam screen, abort kicker, and polarimeter. To perform the thermal analyses, the resistive wall loss on individual components is calculated with CST and the synchrotron radiation (if exists) is evaluated using SynRad. These losses, along with realistic boundary conditions are then fed to ANSYS to determine the temperature distribution.

INTRODUCTION

The EIC [1–3] is one of the most challenging accelerator machines to be designed, and upon completion, will collide a polarized beam of hadrons with electrons. The Electron Storage Ring (ESR) is designed to operate at an average beam current up to 2.5 A within 1160 bunches with a ~ 7 mm rms bunch length for the worst case scenario in terms of thermal heating. Likewise, the Hadron Storage Ring (HSR) will accumulate an average current of 0.69 A within 290 bunches with a 60 mm rms bunch length for the worst-case thermal heating. The intense beams of the ESR and HSR produce a large amount of beam-induced resistive wall losses that can lead to overheating of the EIC vacuum chamber components. The impedance analysis of ESR and HSR vacuum chamber components from both the single-bunch and multi-bunch perspectives is ongoing. Preliminary impedance analysis can be found in [4–6]. Our earlier paper on beam-induced heating and thermal analysis can be found in [7], where we presented heating and thermal analysis for ESR BPM, ESR standard RF shielded bellows and gate valve, and the HSR stripline injection kicker. In this paper, we discussed other components such as the ESR Large Angle Bremsstrahlung Monitor (LABM), HSR cryo-cooled BPM button assembly, HSR beam screen, abort kicker, and polarimeter.

To perform thermal analysis, the resistive wall losses for individual components are calculated using the 3D electromagnetic code CST [8]. The synchrotron radiation, mainly for ESR components, is evaluated using the SynRad code. The results are fed into another program, ANSYS [9], as are appropriate boundary conditions such as circulating water, heat conduction from room temperature to cryogenic components, etc. We adopted this method for thermal analysis as it was proven to align with the experimental data while testing the APS-U stripline kicker at the NSLS-II facility.

ESR COMPONENTS

Most of the ESR vacuum chamber components have an elliptical profile with 80 mm horizontal and 36 mm vertical dimensions. These components experience maximum local heating with an average beam current of 2.5 A (27.6 nC per bunch) from 1160 bunches that are only 7 mm long. Therefore, we used these beam parameters to calculate the local metallic losses for all the ESR components. As we stated earlier, the thermal analysis for some ESR components can be found in Ref. [7], where we showed that most of the ESR components require active water cooling. We re-ran thermal simulations of these ESR components by increasing the water flow rate from 6 gallons per minute to 8 gallons per minute. Despite the increased flow rate, the reduction in the maximum temperature was minimal. Here we report the RW loss for the ESR LABM, Figure 1 (a), for which the thermal analysis needs to be completed.

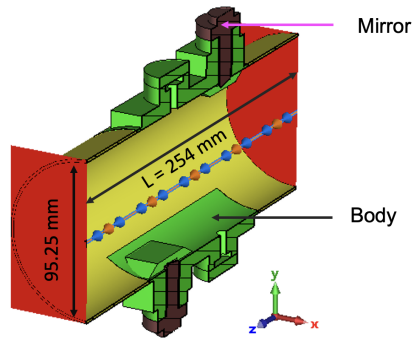
The ESR LABM will be placed upstream of the interaction region to measure the quality of the e-beam. For now, we consider a circular profile having an inner diameter of 95.25 mm. We performed CST simulations for this LABM by treating all the materials as annealed copper. The RW losses on individual components of ESR LABM seem to be manageable and are listed in Figure 1 (b). In the following section, we report the heating and thermal analysis for the HSR components.

HSR COMPONENTS

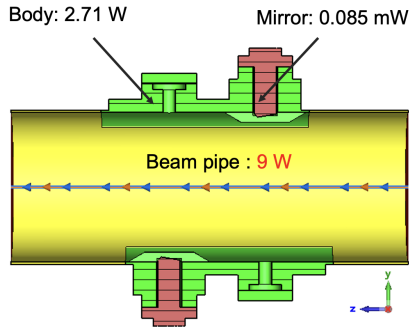
The EIC Hadron Storage Ring (HSR) will accumulate an average current of 0.69 A from 290 bunches with a 60 mm rms bunch length for the worst-case scenario in terms of resistive wall heating. However, it will have 1 A with 1160 bunches for the high luminosity case. Based on the energy, the hadron beam can have a large radial offset of ± 20 mm. This large radial offset is one of the main concerns from an overheating standpoint. The beam-induced heating and corresponding thermal analysis will be performed for

* Work supported by Brookhaven Science Associates, LLC under Contract No. DE-SC0012704 with the U.S. Department of Energy.

[†] msangroul@bnl.gov



(a)



(b)

Figure 1: ESR LABM section showing the (a) internal structure, and (b) the values of RW losses.

all the HSR vacuum chamber components including the collimator, bellows, and others. Here, we focus on the thermal analyses for the HSR components including the cryo-cooled BPM, the beam screen, the dual plane polarimeter, and the abort kicker.

HSR Cryo-cooled BPM Bellows Assembly

The geometry of the HSR cryo-cooled BPM bellows assembly is shown in Figure 2 (left), along with the BPM button module (right). The main concerns for this assembly are the overheating of the BPM button and thin flexible rf-fingers due to lateral beam offsets. The concern regarding BPM button heating resulted in the current corner button design. A paper on the design evolution of the HSR BPM button is in progress. The BPM button has a curved surface following the HSR beam-screen profile. The button is made of stainless steel and has a copper coating to reduce RW loss and amorphous carbon on top of the copper to reduce SEY. Heating of the BPM button is mainly due to the RW loss and heat conduction via cryogenic cable from room temperature. We discuss these two cases separately in the following sub-sections.

Heating due to RW loss The heating due to RW losses is calculated using the HSR Beam parameters; 60 mm rms bunch length, 30.5 nC charge per bunch, and from 290 bunches. In addition, we consider a horizontal beam offset

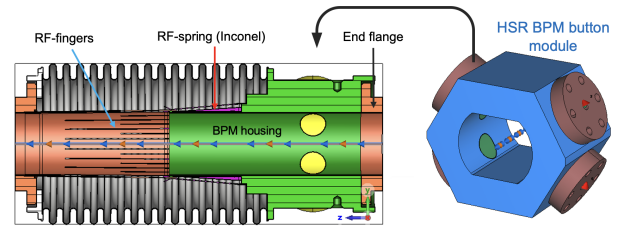


Figure 2: HSR BPM bellows assembly (left), and the BPM button module only (right).

of 23 mm, and a vertical offset of 2 mm for the worst-case scenario for this particular geometry. Here we used a 23 mm horizontal offset which is the sum of the radial offset (20 mm) and mechanical tolerance (3 mm) associated with the bellows geometry. The 2 mm vertical offset is due to beam oscillation at the injection.

The RW losses to the BPM button geometry are highly asymmetric due to lateral beam offsets. Even for the on-axis beam, the losses are asymmetric around the housing of the BPM as shown in Figure 3 (a) left. Here, we evaluated the piece-wise loss for the simplified BPM housing, Figure 3 (a) right, by slicing it into 18-pieces, each of which subtends 20° at the center. Therefore, to model a more accurate thermal analysis, the RW losses for the BPM button and the button housing have been calculated separately. Figure 3 (b) depicts the values of RW loss on the BPM buttons due to the horizontal beam offset of 23mm, and vertical offset of 2 mm. For the housing, we evaluated the piece-wise RW loss with these offsets.

After evaluating the RW loss for housing and BPM buttons using room temperature conductivity, we scaled them to cryogenic temperature values by considering the values of the Residual Resistance Ratio (RRR), Anomalous Skin Effect (ASE), and magnetoresistance effect. In the following subsection, we briefly discuss heating due to thermal conduction from cryo-cable.

Heating due to Thermal Conduction The inevitable heat conduction through cryogenic cables from room temperature ($\sim 300\text{K}$) to cryogenic temperature ($\sim 4\text{K}$) is another big source for the heating of the HSR BPM button. Figure 4 (a) shows a CAD model of the HSR cryostat and Figure 4 (b) shows the cryo-cable designs connected to the BPM button's feedthrough. To reduce the amount of heat conduction from these cables, we plan to use the magnet heat shield (50 – 80) K as a heat sink similar to what we have done for RHIC.

We investigated the heat conduction using two different cryo-cable dimensions, the smaller cable diameter has a diameter of 0.090 inches while the larger cable has a diameter of 0.141 inches. Both cables have their own pros and cons. The evaluated heat conduction data is compared between three facilities; EIC, RHIC, and LHC. EIC showed the lowest total heat conduction among all while incorporating the smaller cable (0.090-inch). Therefore, we used this smaller cryo-cable dimension for our thermal analysis. The choice of

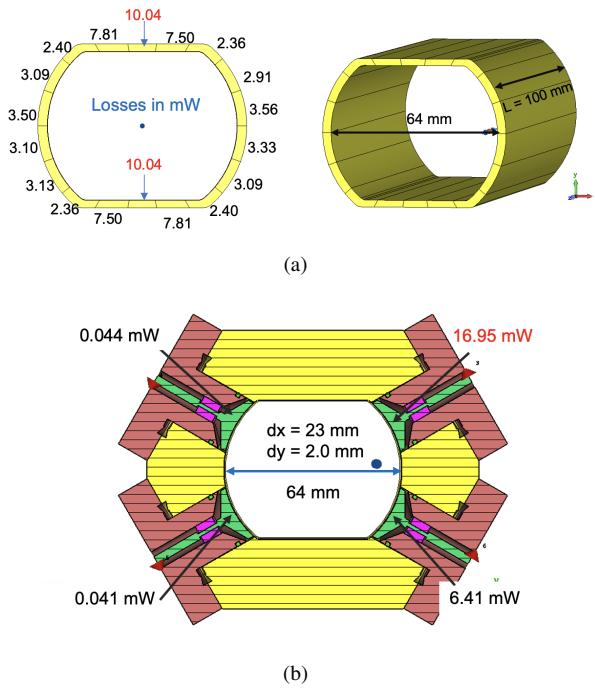


Figure 3: (a) Piece-wise RW loss (mW) due to on-axis beam around the BPM housing (left), simplified model of HSR BPM housing sliced into 18-pieces (right), and (b) RW loss on the BPM buttons due to offset beam.

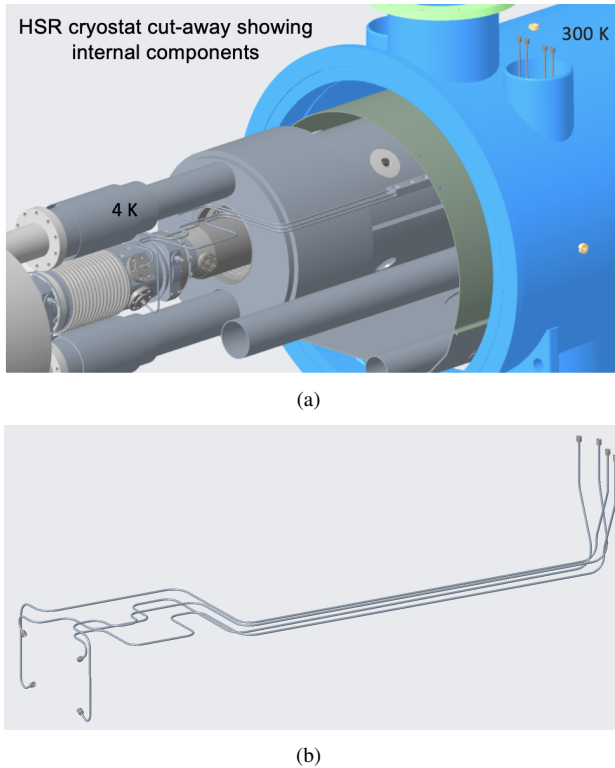


Figure 4: HSR cryostat (a) showing the internal structure, and (b) BPM cryo-cables (length of each cryogenic signal cable is about 1.2 m).

the cable, however, is still under consideration. The detailed thermal analysis of the HSR cryo-cooled BPM can be found in [10].

Thermal Analysis After evaluating the RW loss and heat conduction from the cryogenic cables, we performed an ANSYS simulation including the energy deposition from the RF voltage. Simulation showed that BPM's stem and button surface receive the higher temperature as shown in Figure 5(a). The temperature of the button surface and stem varies with the peak voltage of the BPM, which ultimately depends on the position of the lateral beam offset. Figure 5(b) shows the variation of temperature of the button stem (blue curve), and the button surface (orange curve) along with the peak voltage signal. The highest temperature is found to be 39 K for both the stem and button surface when considering the maximum peak voltage of ~ 82 V at the worst-case beam offsets (horizontal offset $r_x = 23$ mm and the vertical offset $r_y = 2$ mm), Figure 5(c). Our goal is to keep the BPM button housing temperature < 30 K. We are investigating if there is room to further lower the temperature.

HSR Beam Screen

The simplified geometry of the HSR beam screen is shown in Figure 6. The process of welding the beam screen removes part of the copper layer and exposes a thin longitudinal stainless steel strip which is ~ 2 mm wide. We wanted to keep this steel strip in the middle of the top flat surface as shown in Figure 6 (a), right. At first, the vendor denied this possibility, assuming the complexity it can introduce in fabrication. They suggested placing the strip on the curved wall, at 11 mm down from the flat top, as shown in Figure 6 (a), left.

Because the location of the strip is very close to the beam in the worst-case transverse offset, the RW loss on the steel strip is very high, as shown in the dark blue curve in Figure 6 (b). Therefore, we asked the vendor if they could move up the strip location near the corner between the flat top and curved surfaces. They agreed to move the strip slightly up so that it would be 6 mm down from the top. Now, they feel confident in fabricating the beam screen with the steel strip on the flat top surface as shown in Figure 6 (a), right.

We compared the RW loss on the stainless steel strip by placing it at the three different locations stated above in Figure 6 (b). Comparison shows the lower value of the RW heating for the H-offset beam (> 12 mm) when the strip is at the flat wall, the green curve in Figure 6 (b). However, for the beam offset lower than 11 mm, the losses are higher on the strip for this case. For the EIC, the hadron beam has nominal offsets greater than 10 mm, hence placing the strip at the center seems an attractive option.

After finalizing the strip location on the beam screen, we performed simulations for a complete beam screen geometry by adding all the components such as longitudinal slots, cooling channel, and outer jacket. Figure 7(a) shows a cross-sectional sketch of a complete beam screen while Figure 7(b) shows the corresponding CAD model showing all the geometries. In addition, we added a stainless steel

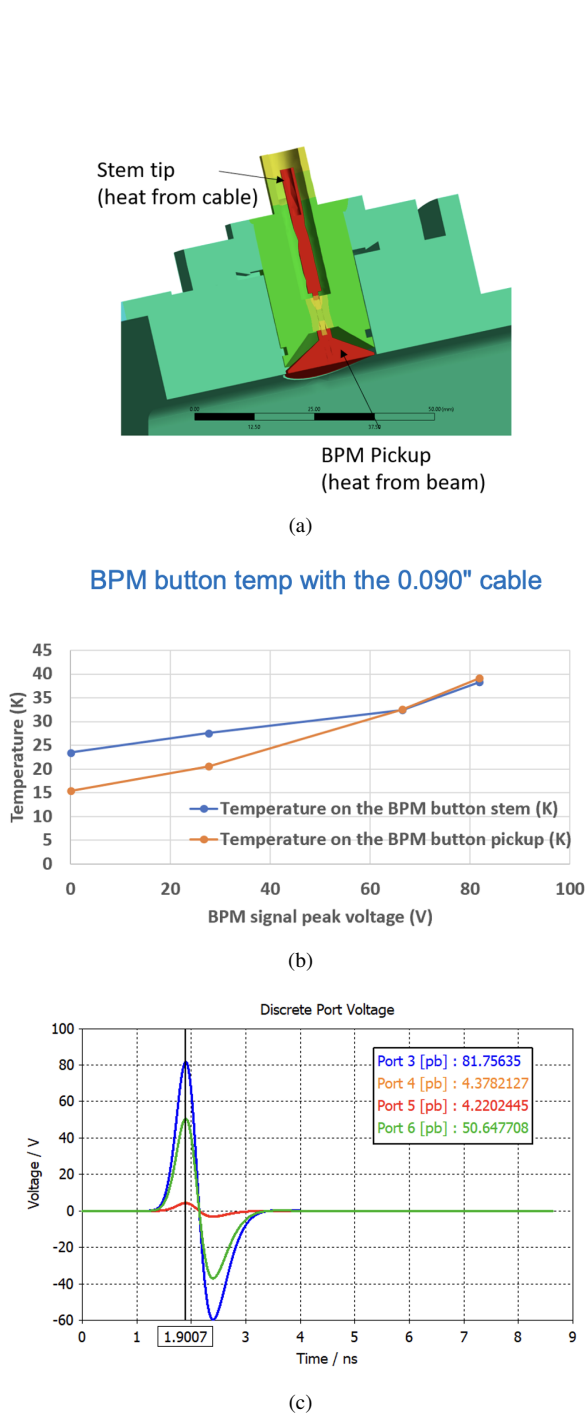


Figure 5: HSR BPM showing (a) thermal distribution, (b) variation of temperature for the BPM stem and button with peak signal voltage, and (c) simulation plot showing peak voltages for the worst case offset horizontal offset of $r_x = 23$ mm and vertical offset of $r_y = 2$ mm. We consider the peak voltage due to port 3 in our simulation.

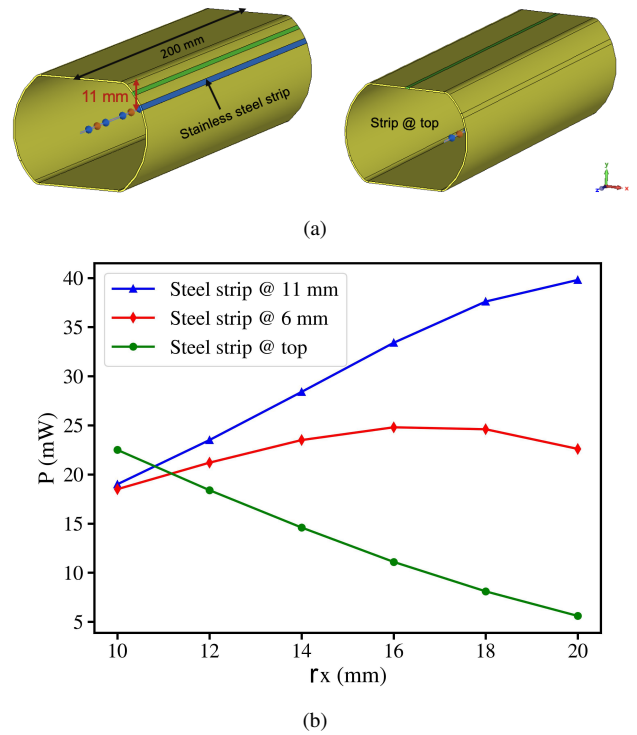


Figure 6: (a) HSR BPM screen geometry without longitudinal slots with the stainless steel strip on the curved wall (left), and top flat (right). (b) RW loss comparisons for the stainless steel strip only with the horizontal (radial) beam offset r_x , at three different strip locations on the screen.

outer layer on the copper beam screen for simulation as the actual screen has a copper plating on top of stainless steel. In reality, the beam screen has three layers; amorphous carbon (aC), copper, and stainless steel. The thickness of the aC is on the order of \sim nano-meters, and our simulation shows it has a negligible impact on the RW loss contribution.

We evaluated the RW loss for the HSR beam screen using room temperature conductivity along with the horizontal and vertical beam offsets. Then, we scaled the corresponding loss to cryogenic temperature by including the effect of residual resistance ratio ($RRR = 10$) for copper, magneto-resistance effect (MR), and anomalous skin effect (ASE). Figure 7(c) depicts the variation of the RW loss per unit length with horizontal and vertical offsets at the dipole (arc) section of the HSR. As guidance, we assume the upper limit for total power loss is 0.5 W/m. Based on this, Figure 7(c), informs that for the on-axis beam, the maximum allowable vertical offset is ~ 2 mm in this particular section. The detailed calculation of the impedance and RW loss on the HSR beam screen can be found in [11]. In practice, the cryogenic group will provide the heat load budget for the cooling circuit.

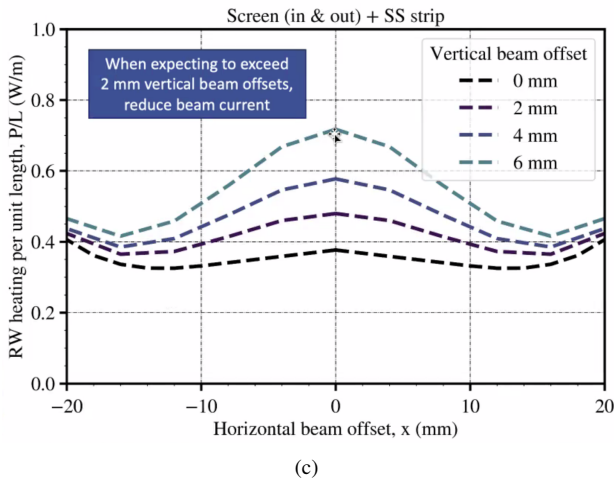
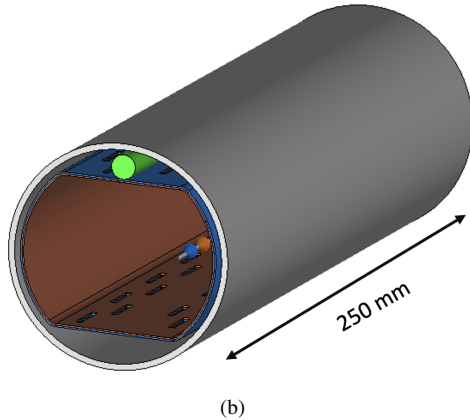
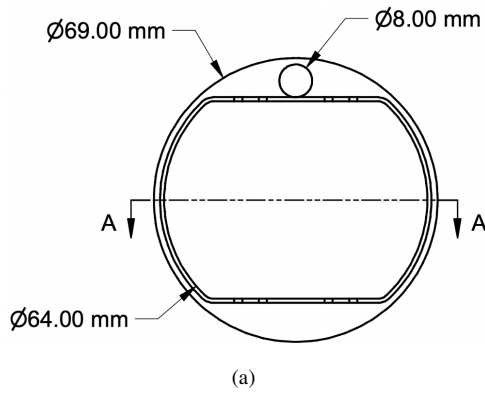


Figure 7: Complete geometry of HSR beam screen, (a) cross-sectional sketch, (b) corresponding CAD design showing the He-cooling channels (green), inner copper layer with slots (orange) and outer steel layer (blue), and (c) RW loss per unit length with horizontal and vertical beam offsets.

HSR Dual Polarimeter

Another important HSR component with complicated geometry is the HSR dual polarimeter, which is required in order to measure horizontal and vertical polarization. Figure 8 (a) shows a CAD model for this polarimeter along with two internal horizontal targets. In reality, we will have two additional vertical targets. These targets are made of

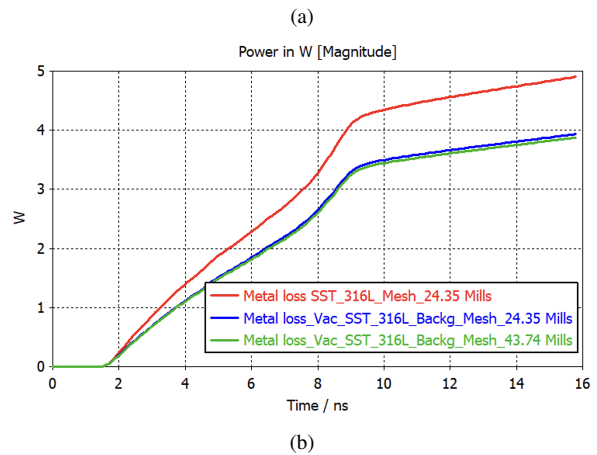
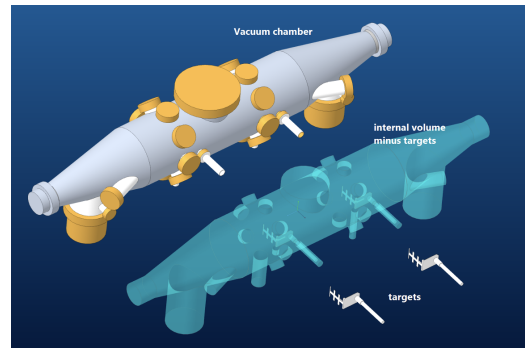


Figure 8: (a) CAD design of the HSR dual polarimeter with two horizontal targets, and (b) the corresponding resistive wall loss comparison with mesh resolution.

amorphous carbon (graphite), and the vacuum chamber is made of stainless steel.

We performed CST simulation to evaluate the RW loss for this polarimeter without including any targets. Because the geometry is complicated having multiple ports and two large pump ports, simulation with actual materials did not easily converge. Hence, we used the vacuum volume for simulation by defining stainless steel 316L as a background material. In this case, the RW loss converges between two mesh settings, the dark blue and green curves in Figure 8(b). Resistive wall losses usually get saturated after some time, but here it is continuously increasing for the HSR polarimeter and is still under investigation. We plan to re-run simulation for this geometry by incorporating the RF shielding on the two large vacuum ports and with targets. In addition, thermal analysis needs to be completed.

HSR Abort Kicker

The next component we investigated was the HSR abort kicker as we observed unusual heating and misfiring on the current RHIC abort kicker. The EIC HSR abort kicker design is based on the existing RHIC abort kicker [12, 13]. Figure 9 (a) shows a CAD model of a single module of the HSR abort kicker we used for simulation. In practice, we have five abort kicker magnet assemblies in a row. The abort kicker consists of ferrite (CMD10) blocks, two eddy current strips

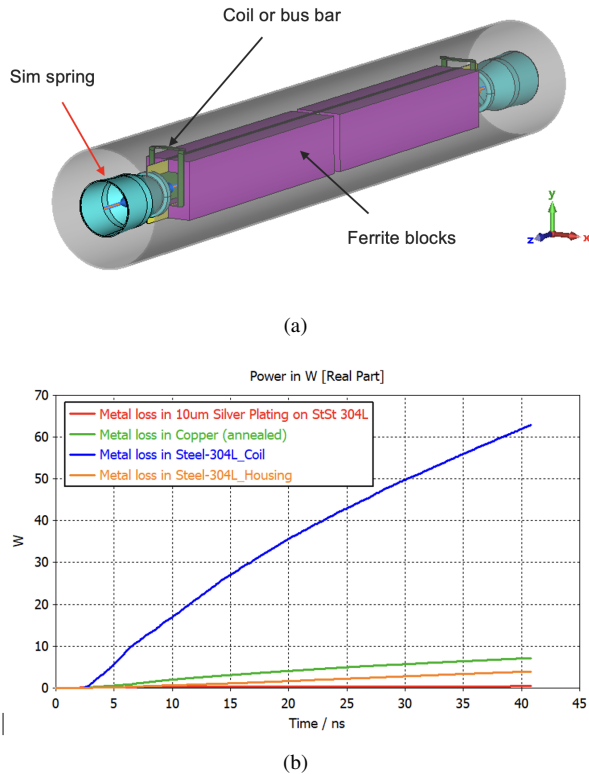


Figure 9: (a) CAD model of the HSR abort kicker, and (b) the corresponding resistive wall loss for different components. We used $\epsilon_r = 12$, and $\mu_r = 1$ for the ferrite in this simulation.

made out of copper, and a coil along with its entire housing made of stainless steel 304L. The sim-spring is made out of 10-micron silver plated stainless steel.

We performed CST simulation for the HSR abort kicker for which the RW loss is shown in Figure 9 (b). Here, we used $\epsilon_r = 12$, and $\mu_r = 1$ for the ferrite. The RW losses for the individual components of this kicker are also monotonically increasing, especially for the coil (dark blue curve in the Figure 9 (b)), which could be due to oscillating wakefield because of large transverse opening. We plan on including the exact properties of the ferrite and doing thermal analysis in the future.

HSR BPM Bellows with Pumping Ports

The final HSR component that we discuss is the HSR bellows with pumping ports. Figure 10 shows a CAD design in cut view of an HSR bellows with pumping ports. The pumping ports have RF slots to shield the low-frequency electromagnetic wave propagation. The geometry of the HSR bellows is similar to that of the HSR BPM bellows assembly, shown in Figure 2.

Simulations were performed for this bellows with pumping ports to evaluate RW loss. The localized losses, also listed in Figure 10, are comparable to that of the BPM bellows assembly when we normalized to the length of corresponding geometries. The thermal analysis to check if

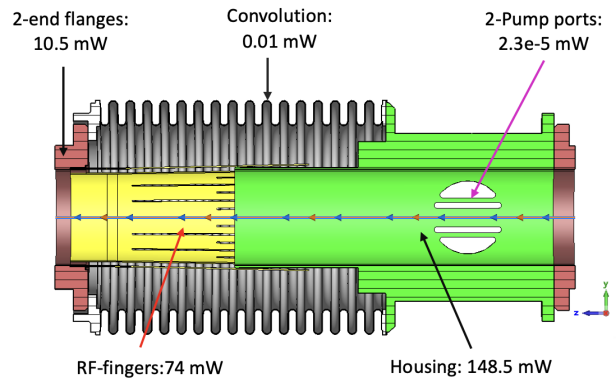


Figure 10: HSR bellows with pumping ports showing the resistive wall loss on its components.

the thin flexible RF fingers can tolerate the beam offsets is ongoing.

SUMMARY

In this report, we presented our beam-induced heating analysis for several EIC vacuum chamber components. We believe that 2.5 A average current for the Electron Storage Ring is achievable by incorporating active water cooling. The simulated HSR BPM Button temperature is $T \sim 40$ K. This temperature value is acceptable since the button surface area is small. The temperature elevation includes beam RW heating, heat conduction from the cable attached to the room temperature connector, resistive heating of the cable from the BPM signal, and electron cloud heating. The goal to keep the housing $T < 30$ K is achieved to limit the desorption of condensed gas. In addition, we reported RW loss for other HSR components such as the HSR beam screen, abort kicker, dual polarimeter, and bellows with pumping ports. We will continue our thermal analysis for both the ESR components and HSR components in the future.

REFERENCES

- [1] Electron-Ion Collider. <https://www.bnl.gov/eic/>
- [2] C. Montag, E. C. Aschenauer, *et al.*, “Design Status Update of the Electron-Ion Collider,” in *Proc. IPAC’21*, Campinas, Brazil, May 2021, pp. 2585–2588. doi:10.18429/JACoW-IPAC2021-WEPAB005
- [3] F. Willeke and J. Beebe-Wang, “Electron Ion Collider Conceptual Design Report,” 2021. doi:10.2172/1765663
- [4] A. Blednykh *et al.*, “An Overview of the Collective Effects and Impedance Calculation for the EIC,” in *Proc. IPAC’21*, Campinas, Brazil, May 2021, pp. 4266–4269. doi:10.18429/JACoW-IPAC2021-THPAB238
- [5] G. Wang, M. Blaskiewicz, A. Blednykh, and M. P. Sangroula, “Studies of the Short-Range Wakefields for the Electron Storage Ring in the Electron Ion Collider,” in *Proc. IPAC’21*, Campinas, Brazil, May 2021, pp. 2675–2678. doi:10.18429/JACoW-IPAC2021-WEPAB032

- [6] A. Blednykh *et al.*, “Impedance Optimization of the EIC Interaction Region Vacuum Chamber,” in *Proc. IPAC’21*, Campinas, Brazil, May 2021, pp. 4270–4273.
doi:10.18429/JACoW-IPAC2021-THPAB239
- [7] M. P. Sangroula *et al.*, “Localized Beam Induced Heating Analysis of the EIC Vacuum Chamber Components,” in *Proc. NAPAC’22*, Albuquerque, USA, 2022, pp. 833–836.
doi:doi:10.18429/JACoW-NAPAC2022-WEPA85
- [8] CST Studio Suite. <https://www.3ds.com/products-services/simulia/products/cst-studio-suite/solvers/>
- [9] ANSYS Software. <https://www.ansys.com/>
- [10] F. Micolon, D. Gassner, C. Hetzel, I. Pinayev, M. Sangroula, and S. Verdu-Andres, “Thermal simulation of the HSR arc BPM Module for EIC,” Brookhaven National Lab.(BNL), Upton, NY (United States), Tech. Rep., 2023.
- [11] S. Verdu-Andres and M. Sangroula, “Beam-induced Heat Deposition in the EIC HSR Screen,” Brookhaven National Lab.(BNL), Upton, NY (United States), Tech. Rep., 2023.
- [12] H. Hahn, A. Dunbar, C. Pai, R. Sanders, N. Tsoupas, and J. Tuozzolo, “The rhic beam abort kicker system,” in *Proceedings of the 1999 Particle Accelerator Conference (Cat. No. 99CH36366)*, IEEE, vol. 2, 1999, pp. 1100–1102.
- [13] W. Fischer, “RHIC beam abort system upgrade options,” Brookhaven National Lab.(BNL), Upton, NY (United States), Tech. Rep., 2019.